Available online at www.sciencedirect.com
ScienceDirect
Journal of Sound and Vibration 308 (2007) 548–562
JOURNAL OF SOUND AND VIBRATION
www.elsevier.com/locate/jsvi

Effects of key parameters on energy distribution and kinetic characteristics in collision of bar and beam

T. Narabayashi[a,*], Kazuo Shibaike[b], A. Ishizaka[a], K. Ozaki[c]

[a]*Department of Precision Engineering, School of Engineering, Tokai University, 1117, Kitakaname, Hiratsukasi, Kanagawa, Japan*
[b]*TOSHIBA TEC Gotanda 2-17-2, Shinagawa-ku, Tokyo, Japan*
[c]*Department of Primemover Engineering, School of Engineering, Tokai University, 1117, Kitakaname, Hiratsukasi, Kanagawa, Japan*

Accepted 3 May 2007
The peer review of this article was organised by the Guest Editor
Available online 10 July 2007

Abstract

Elastic-collision problems are the foundations of all collision problems, and a bar and a beam can represent a typical and simple structure. However, the elastic collision of a bar and a beam is a complicated phenomenon. The purpose of this research is to clarify the relationship between the principal parameter and the kinetic characteristics that influence this complicated elastic collision phenomenon, and to explain these on the basis of an impact force waveform, the apparent coefficient of restitution, and energy distribution. We employed an analysis method in which the impact force assumes an exponential function for the basic equation of the one-dimensional elastic vibration corresponding to the longitudinal vibration of the bar and the lateral vibration of the beam, and in which the force satisfies the condition of continuity of the displacement. In the experiment, assuming flat-surface contact, we directly detected collision phenomenon electrically using PZT pasted onto the end surface of the collision bar. On the basis of this study, the key parameter in the above-mentioned collision phenomenon is clarified, and an energy distribution situation and the influence of each parameter can now be considered for arbitrary combinations of the bar and beam. Furthermore, it is assumed that there is a correlation among the energy state after collision between a bar and a beam, the restitution state and the sound generated when a beam and a bar collide. Therefore, it is important to analytically study the effect of key parameters on various energy states. Thus, as our principal result, the complicated motion of a system involving an intermittent collision phenomenon namely, an elastic bar and an elastic beam supported at both ends, was clarified theoretically and experimentally.
© 2007 Elsevier Ltd. All rights reserved.

1. Introduction

When a bar collides perpendicularly with a beam, longitudinal vibration is generated in the bar, while lateral vibration is generated in the beam. Both the bar and beam have a definite elastic property; however, collision phenomena between a bar and a beam are very complicated, since their elastic properties influence each other. Regarding collision, particularly lateral collision, of a beam having a typical simple structure, Timoshenko reported analytical results for a falling steel ball many years ago [1]. Majima and Nishida carried out a drop test of a weight and reported intermittent-type collision within a short time [2]. With the advancement of

*Corresponding author.
E-mail address: nara@keyaki.cc.u-tokai.ac.jp (T. Narabayashi).

0022-460X/$ - see front matter © 2007 Elsevier Ltd. All rights reserved.
doi:10.1016/j.jsv.2007.05.008

measurement instruments, the number of reports on measurement methods using strain gauges and piezoelectric elements (PZTs) has been increasing [3–5]. However, detailed discussion has not been carried out on intermittent-type collision between a bar and a beam. At the ATEM' 99 and ICEM12 International Conference, the authors demonstrated and reported the effectiveness of (1) the analytical method based on a one-dimensional fundamental equation on collision phenomena between a bar and a beam to satisfy the condition of continuity and (2) an experimental method of observing the collision phenomena [6] and restitution characteristics [7] in terms of electrical characteristics. In this analytical method, rotatory inertia and shear deformation of the beam are disregarded for simplicity. In addition, assuming impact force to be an exponential function of time [8,9], the equations are solved such that the condition of continuity between the bar and the beam are satisfied, in order to clarify the complicated motion phenomena during collision.

In this paper, a both-ends-supported beam, which is easily realized as a supporting condition, is used, and PZT is pasted onto the end surface of the colliding bar and the collision phenomena are observed in terms of electrical characteristics. A comparative study was also carried out on the key parameters in the analysis and experiment, while changing collision position. Since the experimental and theoretical results generally were in good agreement, we concluded that both our theory and experimental method are effective even under the condition that collision position changes. Furthermore, the changes of in the kinetic characteristics of the bar and beam are discussed from the viewpoint of changes in collision position, restitution characteristics and energy distribution.

2. Setting problem and outline of fundamental equations for analysis

A case in which an elastic bar (length: l_1, cross-sectional area: A_1, density: ρ_1, longitudinal elastic coefficient: E_1, velocity of longitudinal wave: c_1) collided perpendicularly with an elastic beam (l_2, A_2, ρ_2, E_2 and c_2) at the center of a beam or at a position l_p from the center in the supported-end direction, at an initial velocity of V, is considered (Fig. 1). The time at which the bar collides with the beam is assumed to be the origin of time (t).

2.1. Equation of motion for center of gravity of bar

Assuming impact force $P(t)$ is applied to the end of the bar in the leftward direction due to collision, the center of gravity of the bar $U(t)$ is obtained by integrating under the initial condition of $U = 0$ and $\mathrm{d}U/\mathrm{d}t = V$ at $t = 0$:

$$\rho_1 l_1 A_1 \frac{\mathrm{d}^2 U(t)}{\mathrm{d}t^2} = -P(t). \tag{1}$$

2.2. Equation of motion and elastic displacement of bar in collision

Impact force $P(t)$ is applied to the end of the bar and the bar is subjected to elastic deformation. Assuming the elastic deformation of the bar end to be $u_1(t)$, the equation of motion is

$$\frac{\partial^2 u_1(t)}{\partial t^2} = c_1^2 \frac{\partial^2 u_1(t)}{\partial x^2}. \tag{2}$$

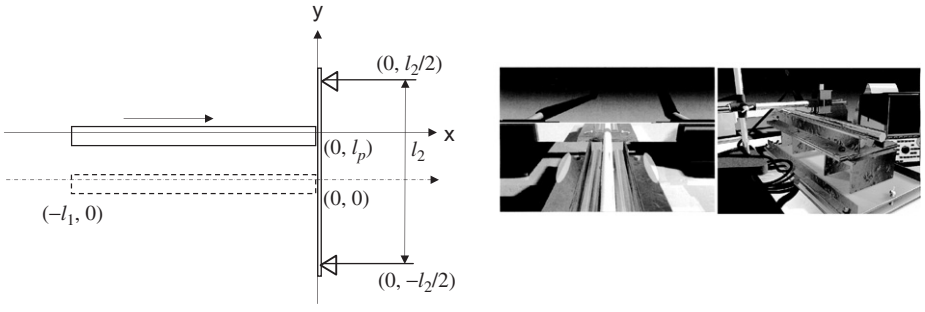

Fig. 1. Bar and beam.

The boundary conditions are expressed as

at $x = 0$,

$$E_1 A_1 \frac{\partial u_1(t)}{\partial x} = \begin{cases} -P(t) & (0 \leqslant t \leqslant T), \\ 0 & (T < t) \end{cases} \tag{3}$$

at $x = -l_1$,

$$\frac{\partial u_1(t)}{\partial x} = 0. \tag{4}$$

The initial condition is given by

$$u_1(t) = 0, \quad \frac{\partial u_1(t)}{\partial t} = 0. \tag{5}$$

The elastic deformation of the bar end can be determined by expanding the equation to an infinite series using the natural angular frequency and the eigenfunction of a both-ends-free bar. The natural angular frequency and eigenfunction of a both-ends-free bar are

$$n_{1v} = v\pi c_1/l_1, \quad U_v = \sqrt{2/l_1}\cos(v\pi x/l_1). \tag{6}$$

The elastic deformation of the bar end is given by

$$u_1(t) = \frac{-2}{\rho_1 A_1 l_1} \sum_{v=1}^{\infty} \frac{1}{n_{1v}} \int_0^t P(\xi) \sin\, n_{1v}(t-\xi)\, \mathrm{d}\xi \tag{7}$$

considering the displacement at $x = 0$. here, v is the mode number.

2.3. Equation of motion and deflection displacement of beam at time of collision

The equation of motion of the beam is expressed by

$$\frac{\partial^2 u_2(t)}{\partial t^2} + \frac{E_2 I_2}{\rho_2 A_2} \frac{\partial^4 u_2(t)}{\partial y^4} = 0, \tag{8}$$

where I_2 is the moment of inertia of area and $u_2(t)$ the deflection displacement of the beam. The deflection displacement of the beam can be calculated by expanding the equation to an infinite series using eigenfunction $W_v(y)$ for both-ends-supported beam:

$$u_2(t) = \frac{1}{\rho_2 A_2} \sum_{v=1}^{\infty} \frac{1}{n_{2v}} W_v(l_\rho)^2 \int_0^t P(\zeta) \sin\, n_{2v}(t-\zeta)\, \mathrm{d}\zeta. \tag{9}$$

Here, assuming the first-mode natural angular frequency of the both-ends-supported beam is n_{21}, $n_{2v} = v^2 n_{21}$ holds. Under this condition, the eigenfunction is expressed as

$$W_v(l_p) = \sqrt{\frac{2}{l_2}} \sin \quad v\pi\left(\frac{l_p}{l_2} + \frac{1}{2}\right) \tag{10}$$

and the deflection displacement of the beam at the time of collision is obtained. Here, l_p/l_2 is the collision position ratio, i.e., the ratio of the distance between the beam center and the collision position to the length between the supported ends.

2.4. Condition of continuity and apparent coefficient of restitution

A case in which a bar collided with a both-ends-supported beam at a position l_p from the center of the beam is considered. The displacement of the bar end is the sum of the displacement of the center of gravity $U(t)$

obtained by integrating Eq. (1) and the elastic displacement of the bar end $u_1(t)$, and is given by

$$U(t) + u_1(t). \tag{11}$$

Next, the displacement of the beam at the collision position, $u_2(t)$, when the impact force $P(t)$ is applied to the collision position, is assumed to be equal to Eq. (11), since the displacement of the bar end and that of the beam at the collision position are equal during collision, and holds

$$U(t) + u_1(t) = u_2(t). \tag{12}$$

Assuming the displacement of the center of gravity of the bar before collision to be U_0 and that added after collision to be U_1, the above equation is expressed Eq. (13):

$$U_0 = Vt = u_2(t) - (U_1 + u_1). \tag{13}$$

Because the left-hand side of Eq. (13) changes linearly with time, the right-hand side should also change similarly. The impact force $P(t)$ is approximated using the following equation such that the right-hand side of Eq. (13) changes as linearly as possible with time, as shown in Fig. 2(b), and both P_1 and μ_1 are adjusted so that the continuity condition of displacement is satisfied:

$$P(t) = P_1 e^{-\mu_1 t}. \tag{14}$$

Once Eq. (14) is determined, both the elastic deformation generated in the bar and the deflection displacement generated at the collision position of the beam can be obtained as infinite series using the eigenfunctions of the bar and beam. Here, the equations of displacement of the bar and beam are obtained as a function of t, in which the mass ratio and natural frequency ratio of the bar and beam are used as parameters and μ_1 as an unknown. By considering the collision position ratio contained in the eigenfunction of the beam, it becomes possible to calculate the motion of the bar and the beam. Based on the equation for the distance between the bar and the beam $(= u_2(t) - \{U(t) + u_1(t)\} > 0)$, it is found that the bar end separates from the beam. Collisions cease at this point, and the bar and beam will not collide again unless the distance between the two becomes 0 before approximately 3/4 of the period of the beam. In this case, the bar and the beam collide only once. In contrast, when they collide n times, they come into contact again at time T_n at which the distance between the bar and the beam is 0 or less. Assuming an impact force expressed by

$$P(t) = P_n e^{-\mu_n (t - T_n)} \tag{15}$$

is applied to the bar, P_n and μ_n are determined such that the condition of continuity is satisfied, and the displacement is calculated for the nth or later collisions. By this procedure, various impact force patterns are obtained under various combinations of the three parameters, i.e., (1) the natural frequency ratio of the bar to the beam n_{11}/n_{21}, (2) the mass ratio of the bar to the beam m_1/m_2 (1 and 2 refer to the bar and beam, respectively), and 3) the collision position ratio (l_p/l_2 where l_p: the distance between the beam center and the collision position and l_2: the length between the supported ends). When the bar and the beam collide n times,

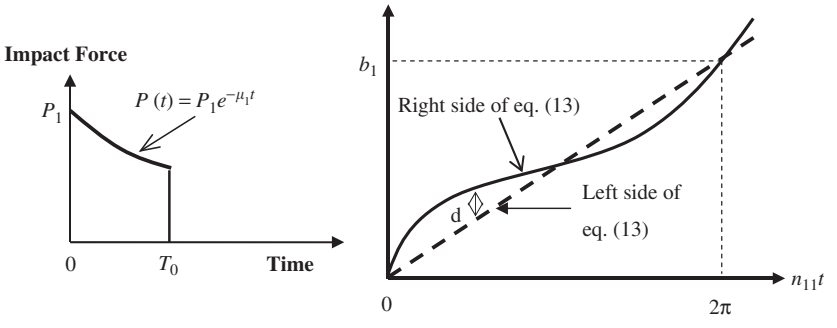

Fig. 2. Approximation of impact force by adjusting μ_1/n_{11} and continuity condition of displacement [8].

the ratio of the velocity of the bar after final collision to the velocity before collision [6] is

$$\frac{1}{V}\frac{\mathrm{d}U_n}{\mathrm{d}t} = \left[1 - 2\pi\left[\sum_{k=1}^{n-1}\left(\frac{a_k}{b_k}\frac{n_{11}}{\mu_k}\left(1 - \mathrm{e}^{-(\mu_1/n_{11})(n_{11}T'_k - n_{11}T_k)}\right)\right)\right.\right.$$
$$\left.\left. + \frac{a_n}{b_n}\frac{n_{11}}{\mu_n}\left(1 - \mathrm{e}^{-(\mu_1 - n_{11})(n_{11}t - n_{11}T_n)}\right)\right]\right]. \tag{16}$$

Here, μ_n/n_{11}, a_n and b_n are the coefficients obtained when the equation is solved so that the condition of continuity is satisfied. Eq. (16) is the ratio of the velocities for multiple collisions and not that of two velocities for a single collision. Therefore, the absolute value of Eq. (16) is defined as the apparent coefficient of restitution in this paper.

2.5. Equations of dimensionless impact force

When μ_n/n_{11}, a_n and b_n, which are obtained by solving the equation to satisfy the continuity condition of displacement, are used, the impact force is nondimensionalized and expressed as

$$P_n = \left|\frac{a_n}{b_n}\right| 2\pi V n_{11}\rho_1 l_1 A_1. \tag{17}$$

In particular, in the equation of impact force for the first collision, $a_n = 1$ and $b_n = b_1$ and

$$P_1 = \frac{2\pi}{b_1} V n_{11}\rho_1 l_1 A_1 \tag{18}$$

holds. Here, the values for a_n and b_n are the same as those in Eq. (16). By carrying out adjustment to satisfy the continuity condition of displacement in Fig. 2, b_1 is obtained, and the dimensionless impact force can be determined.

2.6. Equations related to energy

It is difficult to experimentally study the energy state of a bar and a beam under the condition of no energy dissipation. It is also difficult to construct accurate theoretical equations for the energy state for arbitrary experimental equipment by taking into account energy dissipation. However, it is possible to compare theoretical and experimental results for impact force and restitution conditions. If we can confirm a tendency showing that experimental and theoretical results agree, it is possible to assume that the energy distribution theory based on our principle is valid. In this study, we will attempt to derive an energy equation for studying the effect of key parameters (i.e., natural frequency ratio, mass ratio, collision position ratio) related to the energy distribution in a bar and a beam.

The kinetic energy of the bar before collision comprises: (1) kinetic energy of the bar after collision, (2) elastic energy generated inside the bar, and (3) elastic energy of the beam. Elastic energy is calculated by summing elastic kinetic energy and elastic potential energy. Thus, denoting the collision velocity to be V, velocity of the center of gravity of the bar after collision to be V', elastic displacement of the bar to be u_1 and elastic displacement of the beam to be u_2, the elastic potential energy of the bar is given by

$$EP1 = \frac{A_1 E_1}{2}\int_0^{l_1}\left(\frac{\partial u_1}{\partial x}\right)^2 \mathrm{d}x. \tag{19}$$

The elastic kinetic energy of the bar is given by

$$EK1 = \frac{A_1\rho_1}{2}\int_0^{l_1}\left(\frac{\partial u_1}{\partial t}\right)^2 \mathrm{d}x. \tag{20}$$

The elastic energy of the bar is given by

$$EE1 = EP1 + EK1. \tag{21}$$

The elastic energy of the bar subjected to n collisions can be expressed by Eq. (22) after nondimensionalizing it with the kinetic energy of the bar before collision ($M_1V^2/2$).

$$
\begin{aligned}
EE1 = 8\pi^2 \sum_{v=1}^{\infty} \Bigg[\Bigg[\sum_{k=1}^{n-1} \frac{a_k}{b_k} \frac{1}{v^2 + (\mu_k/n_{11})^2} \Big[v \mathrm{e}^{-\frac{\mu_k}{n_{11}} n_{11}(T'_k - T_k)} \cos\, v n_{11}\big(t - T'_k\big) \\
- v \cos\, v n_{11}(t - T_k) - \frac{\mu_k}{n_{11}} \Big\{ \mathrm{e}^{-\frac{\mu_k}{n_{11}} n_{11}(T'_k - T_k)} \sin\, v n_{11}\big(t - T'_k\big) - \sin\, v n_{11}(t - T_k) \Big\} \Big] \\
+ \frac{a_n}{b_n} \frac{1}{v^2 + (\mu_n/n_{11})^2} \Big\{ v \mathrm{e}^{-\frac{\mu_n}{n_{11}} n_{11}(t_k - T_n)} - v \cos\, v n_{11}(t - T_n) + \frac{\mu_n}{n_{11}} \sin\, v n_{11}(t - T_n) \Big\} \Bigg]^2 \\
+ \Bigg[\sum_{k=1}^{n-1} \frac{a_k}{b_k} \frac{1}{v^2 + (\mu_n/n_{11})^2} \Big[-v \mathrm{e}^{-\frac{\mu_k}{n_{11}} n_{11}(T'_k - T_k)} \sin\, v n_{11}\big(t - T'_k\big) + v \sin\, v n_{11}(t - T_k) \\
- \frac{\mu_k}{n_{11}} \Big\{ \mathrm{e}^{-\frac{\mu_k}{n_{11}} n_{11}(T'_k - T_k)} \cos\, v n_{11}\big(t - T'_k\big) - \cos\, v n_{11}(t - T_k) \Big\} \Big] + \frac{a_n}{b_n} \frac{1}{v^2 + (\mu_n/n_{11})^2} \\
\times \Big\{ - \frac{\mu_k}{n_{11}} \mathrm{e}^{-\frac{\mu_n}{n_{11}} n_{11}(t - T_n)} + v \sin\, v n_{11}(t - T_n) + \frac{\mu_n}{n_{11}} \cos\, v n_{11}(t - T_n) \Big\} \Bigg]^2 \Bigg].
\end{aligned} \tag{22}
$$

The elastic potential energy of the beam is given by

$$
EP2 = \frac{E_2 I_2}{2} \int_{-\frac{l_2}{2}}^{\frac{l_2}{2}} \left(\frac{\partial u_2}{\partial y^2} \right)^2 \mathrm{d}y. \tag{23}
$$

The elastic kinetic energy of the beam is given by

$$
EK2 = \frac{A_2 \rho_2}{2} \int_{-\frac{l_2}{2}}^{\frac{l_2}{2}} \left(\frac{\partial u_2}{\partial t} \right)^2 \mathrm{d}y. \tag{24}
$$

Accordingly, the total elastic energy of the beam is given by

$$
EE2 = EP2 + EK2. \tag{25}
$$

The elastic energy of the beam subjected to n collisions can be expressed by Eq. (26) after nondimensionalizing it with kinetic energy of the bar before collision:

$$
\begin{aligned}
EE2 = 8\pi^2 \frac{\rho_1 A_1 l_1}{\rho_2 A_2 l_2} \sum_{v=1}^{\infty} \sin^2 v\pi \left(P + \frac{1}{2} \right) \Bigg[\Bigg[\sum_{k=1}^{n-1} \frac{a_k}{b_k} \frac{1}{v^4 (n_{21}/n_{11})^2 + (\mu_k/n_{11})^2}, \\
- \frac{\mu_k}{n_{11}} \Big\{ \mathrm{e}^{-\frac{\mu_k}{n_{11}} n_{11}(T'_k - T_k)} \sin\, v^2 \frac{n_{21}}{n_{11}} n_{11}\big(t - T'_k\big) - \sin\, v^2 \frac{n_{21}}{n_{11}} n_{11}(t - T_k) \Big\} \Bigg], \\
\times \Bigg[v^2 \frac{n_{21}}{n_{11}} \mathrm{e}^{-\frac{\mu_k}{n_{11}} n_{11}(T'_k - T_k)} \cos\, v^2 \frac{n_{21}}{n_{11}} n_{11}\big(t - T'_k\big) - v^2 \frac{n_{21}}{n_{11}} \cos\, v^2 \frac{n_{21}}{n_{11}} n_{11}(t - T_k), \\
+ \frac{a_n}{b_n} \frac{1}{v^4 (n_{21}/n_{11})^2 + (\mu_k/n_{11})^2}, \\
\times \Big\{ v^2 \frac{n_{21}}{n_{11}} \mathrm{e}^{-\frac{\mu_n}{n_{11}} n_{11}(t - T_n)} - v^2 \frac{n_{21}}{n_{11}} \cos\, v^2 \frac{n_{21}}{n_{11}} n_{11}(t - T_n) + \frac{\mu_n}{n_{11}} \sin\, v^2 \frac{n_{21}}{n_{11}} n_{11}(t - T_n) \Big\} \Bigg]^2, \\
+ \Bigg[\sum_{k=1}^{n-1} \frac{a_k}{b_k} \frac{1}{v^4 (n_{21}/n_{11})^2 + (\mu_k/n_{11})^2},
\end{aligned}
$$

$$\times\left[-v^2\frac{n_{21}}{n_{11}}e^{-\frac{\mu_k}{n_{11}}n_{11}(T'_k-T_k)}\sin v^2\frac{n_{21}}{n_{11}}n_{11}(t-T'_k)+v^2\frac{n_{21}}{n_{11}}\sin v^2\frac{n_{21}}{n_{11}}n_{11}(t-T_k),\right.$$
$$\left.-\frac{\mu_k}{n_{11}}\left\{e^{-\frac{\mu_k}{n_{11}}n_{11}(T'_k-T_k)}\cos v^2\frac{n_{21}}{n_{11}}n_{11}(t-T'_k)-\cos v^2\frac{n_{21}}{n_{11}}n_{11}(t-T_k)\right\}\right],$$
$$+\frac{a_n}{b_n}\frac{1}{v^4(n_{21}/n_{11})^2+(\mu_k/n_{11})^2},$$
$$\left.\times\left\{-\frac{\mu_n}{n_{11}}e^{-\frac{\mu_n}{n_{11}}n_{11}(t-T_n)}+v^2\frac{n_{21}}{n_{11}}\sin v^2\frac{n_{21}}{n_{11}}n_{11}(t-T_n)+\frac{\mu_n}{n_{11}}\cos v^2\frac{n_{21}}{n_{11}}n_{11}(t-T_n)\right\}\right]^2\Bigg]. \quad (26)$$

According to the law of energy conservation, the relationship below also holds:

$$\tfrac{1}{2}M_1V^2=\tfrac{1}{2}M_1V'^2+EE1+EE2. \quad (27)$$

3. Experimental apparatus and methods

As shown in Fig. 3, the experimental apparatus for the collision of a bar with a both-ends-supported beam was fabricated, and the collision phenomena were detected using a PZT pasted directly onto the end surface of the bar (Fig. 4). In this study, we focused on the measurement of the velocity of the center of gravity of the bar before and after collision, which changes with collision position. Mainly steel and aluminum were used as the beam and bar materials. For the observation of collision phenomena, the rail of the bar was supported at three points in order to achieve planar contact between the bar and the beam, and an adjustment mechanism using screws was attached. To confirm the planar contact, pressure-sensitive paper was used to judge the contact conditions on the basis of the indentation conditions required to avoid inaccurate contact conditions (Fig. 5). Since there were numerous cases in which the restitution conditions change greatly with a slight change in collision position, we ensured that the center of the collision surface of the bar corresponded to the collision

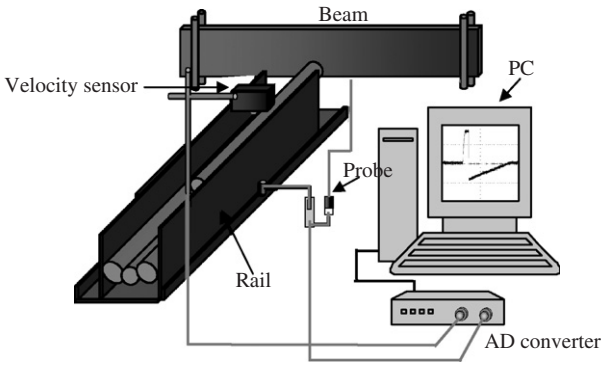

Fig. 3. Experimental setup.

Fig. 4. Bar and PZT.

Fig. 5. Planar and inaccurate contact.

position of the beam. In this study, the apparent coefficients of restitution obtained under planar contacts agree with their theoretical values. A circular bar with PZT on its end is placed on four steel balls set in the grooves of a rail, and the bar is planarly collided with the both-ends-supported beam smoothly at a constant velocity. The collision wave is observed as electrical signals by the time-course change in the potential difference, which is proportional to the applied impact force. The detected signal is attenuated to 1/10 in the probe, then converted to digital signals by an AD converter, and input into the digital oscilloscope or a PC. The input signal is observed and measured on a PC using signal analysis software. The velocity signal is detected using a laser feed monitor, as a velocity measurement unit. The velocities of the circular bar just before and after the bar collides with the beam are converted into the electric signals of the change in potential, which is proportional to the velocity, using a laser beam irradiated from the sensor head. These electric signals are input to the PC and the digital oscilloscope through an AD converter. The results are displayed on a screen. When a bar driven by a striker or by hand undergoes accelerating motion and separates from the striker or hand, the bar undergoes uniform motion. After that, the bar collides with the beam and rebounds in the opposite direction; however, the velocity of the bar decreases due to friction and stops at the stopper. The behavior explained above is observed on the PC screen. The ratio of the velocity of the bar after collision V_2 to the velocity before the collision V_1, V_2/V_1, is calculated using this output, for comparison with theoretical values. Since the bar rebounds, V_2 is a negative value; therefore, the velocity ratio is also negative. The absolute value of this ratio is the apparent coefficient of restitution.

4. Comparison of analytical and experimental results of collision phenomena

4.1. Impact force pattern obtained when mass ratio, natural frequency ratio of bar and beam, and collision position ratio are matched in analysis and experiment

To compare analytical results with experimental results, the three parameters used in the analysis, i.e., (1) mass ratio, (2) natural frequency ratio of the bar and the beam, and (3) collision position ratio, are matched to the values adopted in the experiment as much as possible, and the wave patterns of collision obtained by analysis and experiment are compared. In Figs. 6 and 7 the changes in impact force when the bar collides with the beam at the center of the beam (Fig. 6) or at a position away from the center (Fig. 7) for cases in which $n_{11}/n_{21} = 90.4$ and $m_1/m_2 = 0.49$ (intermittent-type collision) are compared between the experimental and analytical results as examples. The impact force analyzed here is nondimensionalized by solving equations in which the condition of continuity is satisfied. When the bar and the beam collide intermittently and when the bar collides with the beam at a position deviating from the center of the beam, the number of collisions changes in both the experimental (Figs. 6(a) and 7(a)) and theoretical(Figs. 6(b) and 7(b)) results, and the two sets of results show extremely similar patterns with respect to the time axis.

A comparison of the experimental and theoretical results indicates that the impact force patterns are in good agreement even with a change in collision position. When the bar collides with the beam at a position close to the supported end, the number of collisions tends to decrease. This phenomenon is also observed in the impact

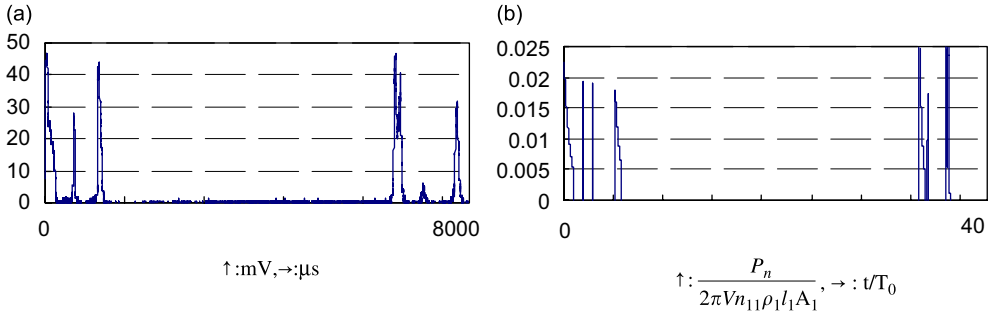

Fig. 6. Impact force pattern ($n_{11}/n_{21} = 90.4$, $m_1/m_2 = 0.49$ $l_p/l_2 = 0$: center position): (a) experimental: aluminum bar (20 mm diameter × 500 mm length)→aluminum beam (10 mm × 50 mm × 646 mm), (b) theoretical.

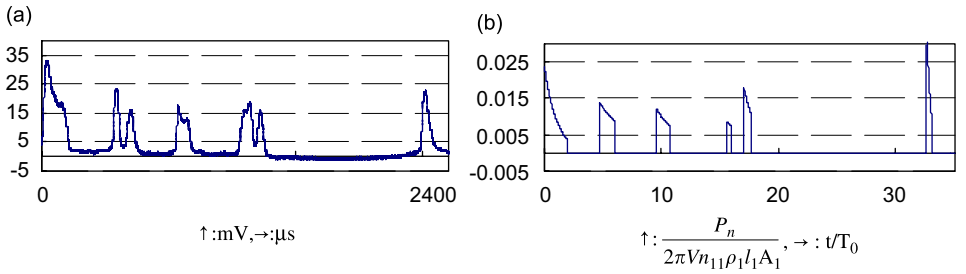

Fig. 7. Impact force pattern ($n_{11}/n_{21} = 90.4$, $m_1/m_2 = 0.49$, $l_p/l_2 = 0.35$ off center position): (a) experimental: aluminum bar (20 mm diameter × 500 mm length) → aluminum beam (10 mm × 50 mm × 646 mm) and (b) theoretical.

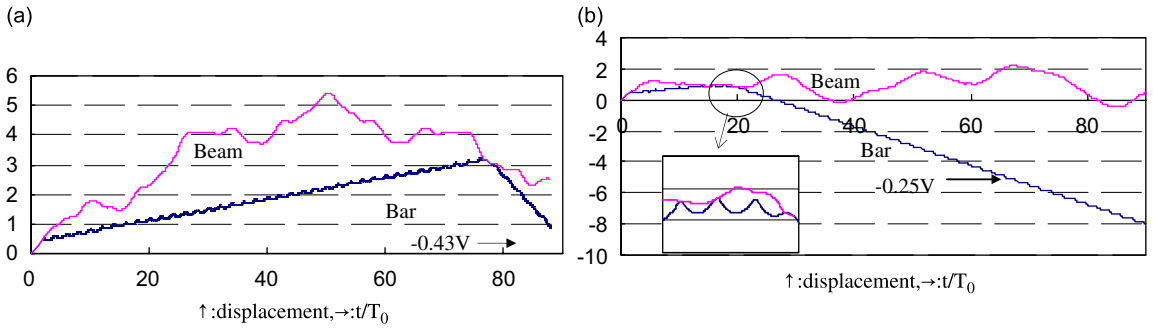

Fig. 8. Theoretical impact motion pattern of bar and beam. ($n_{11}/n_{21} = 98.9$, $m_1/m_2 = 0.16$): (a) $l_p/l_2 = 0$ (center position) and (b) $l_p/l_2 = 0.35$ (off center position).

force patterns obtained by experiment and analysis. The above findings demonstrated that our analytical and experimental methods are effective regardless of the number of collisions and collision position.

4.2. Motion pattern of bar and beam obtained by analysis

Referring to the above experimental results, the motion patterns of the bar and the beam are estimated analytically. In Fig. 8, the upper wavy curve and the lower linearly changing line represent the displacements of the beam and bar with time, respectively, and using same parameters as in Figs. 6 and 7. The vertical axis shows nondimensionalized displacement, and the horizontal axis shows nondimensionalized time. Fig. 8 shows the motion patterns of the bar colliding with the beam at the center of the beam (Fig. 8(a)), at the position $l_p/l_2 = 0.35$ from the center (Fig. 8(b)). The material, shape and support conditions of the bar and beam are identical. For (a) and (b), the bar and the beam collide once, separate and then come into contact again. A comparison of (a) and (b) indicates that the contact conditions of the bar and beam change when the collision position moves from the center of the beam towards the supported end. The number of collisions also changes. In addition, for a bar colliding in the vicinity of the supported end of the beam, the bar collides with the beam only once. It is considered that since the motion of the beam changes greatly, the impact force pattern also changes considerably. Regarding the separation between the bar and the beam, the effect of the propagation condition of the longitudinal waves of the bar is significant [3]. Based on the results of the analysis of this study, when only the collision position is different for the same type of bar and beam under the same collision velocity, the motion of the beam is the main factor governing the number of collisions. Therefore, even when the bar and beam collide at the same velocity, the velocity after the final collision varies depending on collision position.

4.3. Three parameters and apparent coefficient of restitution

The ratio of the velocity of the bar after the final collision to the collision velocity is examined analytically and theoretically with varying (1) natural frequency ratio, (2) mass ratio, and (3) collision position ratio. Fig. 9

shows the results for one collision. The vertical axis indicates the ratio of the velocity of the bar after collision to the velocity before collision (velocity ratio), and the horizontal axis indicates collision position ratio.

Fig. 9(a) shows the change in velocity ratio with changing collision position ratio when the mass ratio is constant and natural frequency ratio varies. When natural frequency ratio decreases, the restitution velocity of the bar increases, leading to an increase in the apparent coefficient of restitution. When the collision position is changed, the velocity ratio takes a constant value up to a certain collision position ratio. However, there is a collision position at which the apparent coefficient of restitution decreases in the vicinity of the supported end. With increasing natural frequency ratio, this collision position approaches the supported end.

However, when the collision position further approaches the supported end, the apparent coefficient of restitution becomes close to 1, i.e., the bar rebounds very well. Fig. 9(b) shows the change in velocity ratio with changing collision position ratio when the natural frequency ratio is constant and the mass ratio varies. When mass ratio increases, the restitution velocity of the bar decreases, leading to a decrease in the apparent coefficient of restitution. With increasing mass ratio, the region in which the velocity ratio is constant narrows. Similar to the case of Fig. 9(a), there is a collision position where the apparent coefficient of restitution decreases, i.e., the restitution velocity of the bar decreases in the vicinity of the supported end. At this collision position, the collision position ratio is approximately 0.4 under various mass ratio conditions. Fig. 10 shows the change in velocity ratio with changing collision position ratio when the natural frequency ratio varies (a) and when the mass ratio varies (b) for intermittent-type collision with mass ratio = 0.49 and natural frequency ratio = 90.4. The plotting point in the figure is an experimental value of the combination, which is similar to the analysis parameter. Unlike in the case of a single collision, the velocity ratio, i.e., the apparent coefficient of restitution is not stable with changing collision position ratio. When natural frequency ratio decreases, the collision position where the restitution velocity of the bar is low is random. In Fig. 10(b), with increasing mass ratio, the region in which the velocity ratio takes a stable value is negligibly small; in other words, the velocity ratio changes significantly even with a slight change in collision position ratio, which is not observed in the

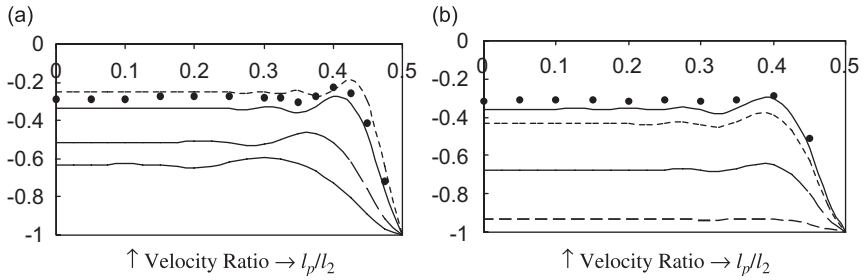

Fig. 9. The ratio of velocity before to velocity after collision V_1/V_2 (single collision): (a) $m_1/m_2 = 0.06$, $n_{11}/n_{21} = 30, 80, 130, 200$ (from the lowest line to order) dot: $n_{11}/n_{21} = 130$ (experimental) and (b) $n_{11}/n_{21} = 90$, $m_1/m_2 = 0.005, 0.03, 0.05, 0.07$ (from the lowest line to order) dot: $m_1/m_2 = 0.07$ (experimental).

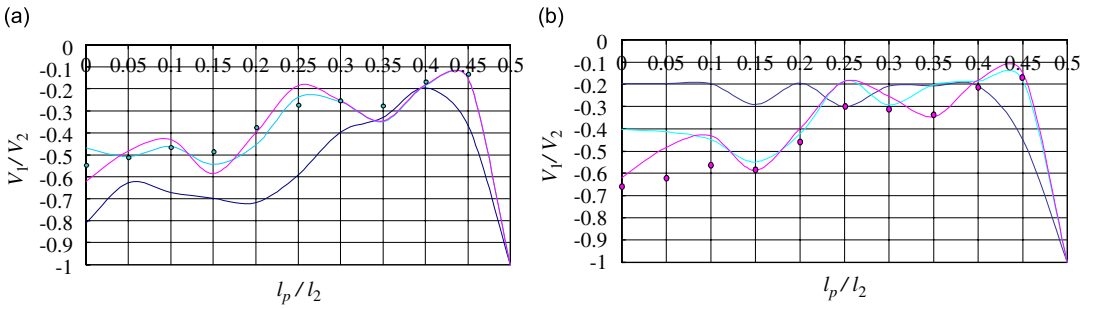

Fig. 10. The ratio of velocity before to velocity after collision V_1/V_2 (intermittent collision): (a) variation with n_{11}/n_{21} ($m_1/m_2 = 0.49$ const.) $n_{11}/n_{21} = 90.25, 90.4, 30$ (from the top line to order at the left side contact point of a line), dot: $n_{11}/n_{21} = 90.25$ (experimental) and (b) variation with m_1/m_2 ($n_{11}/n_{21} = 90.4$ const.) $m_1/m_2 = 0.1, 0.4, 0.49$ (from the top line to order at the left side contact point of a line), dot: $m_1/m_2 = 0.49$ (experimental).

case of one collision. Furthermore, depending on the collision position, the bar rebounds more significantly under a large mass ratio compared with a small mass ratio. Based on the results explained above, the apparent coefficient of restitution, which is relatively stable for a single collision, changes significantly depending on the collision position for intermittent collision.

4.4. Three parameters and energy distribution

Figs. 11 and 12 show the calculated energy distribution states of the bar and the beam subjected to one collision. The left ordinate shows the energy ratio and the right ordinate shows the ratio of restitution velocity to collision velocity. In the case of one collision, the absolute value of the ratio of restitution velocity to collision velocity indicates the coefficient of restitution. The broken line in Figs. 11 and 12 represents the ratio of restitution velocity to collision velocity. As shown in the figure, when the number of collisions is one and the ratio of natural frequencies of the bar and beam is small, the proportion of kinetic energy of the bar is large

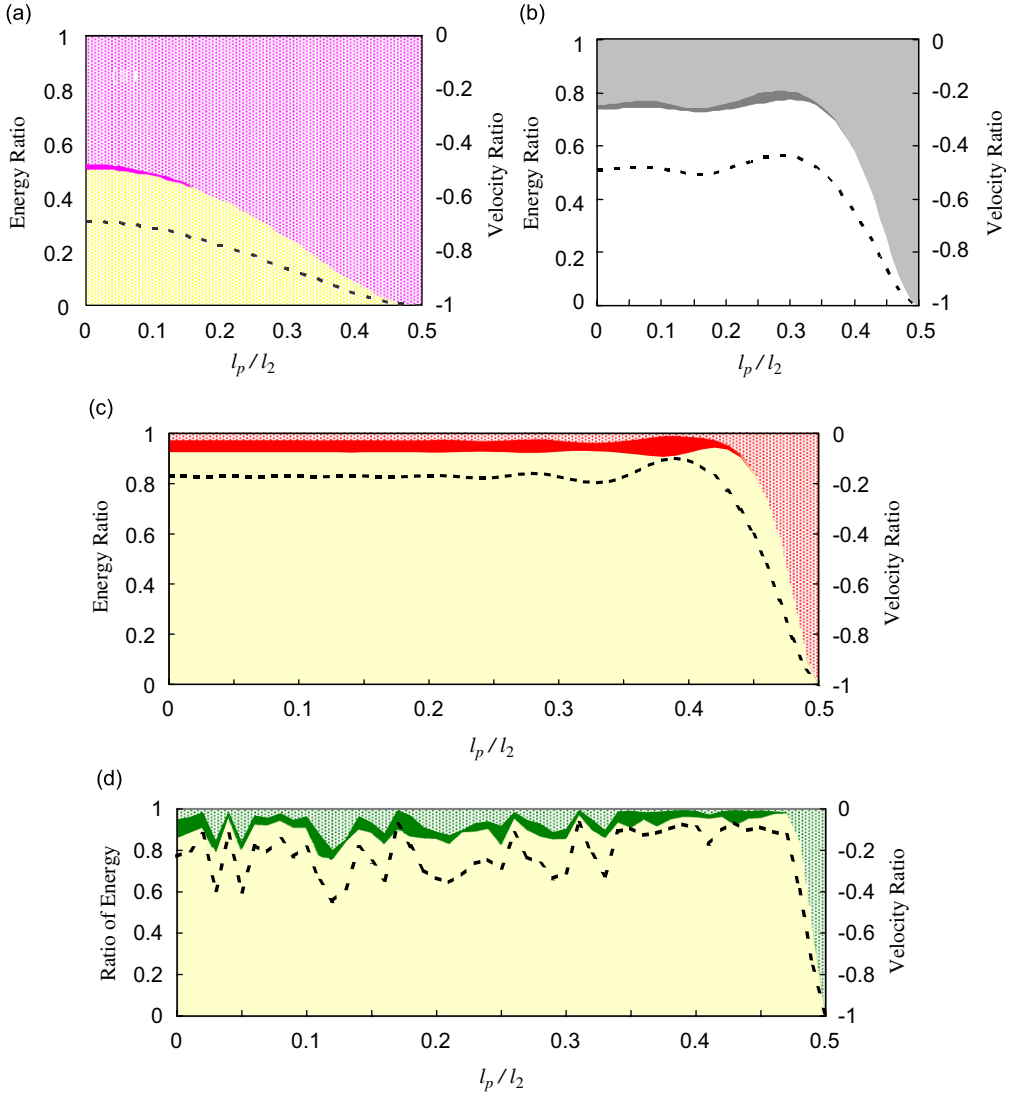

Fig. 11. Changes in natural frequency ratio and energy distribution (theoretical): (a) $n_{11}/n_{21} = 5$, (b) $n_{11}/n_{21} = 25$, (c) $n_{11}/n_{21} = 100$, (d) $n_{11}/n_{21} = 300$, top layer: kinetic energy of bar, mid-layer: elastic energy of bar, bottom layer: elastic energy of beam, dotted line: velocity ratio (theoretical).

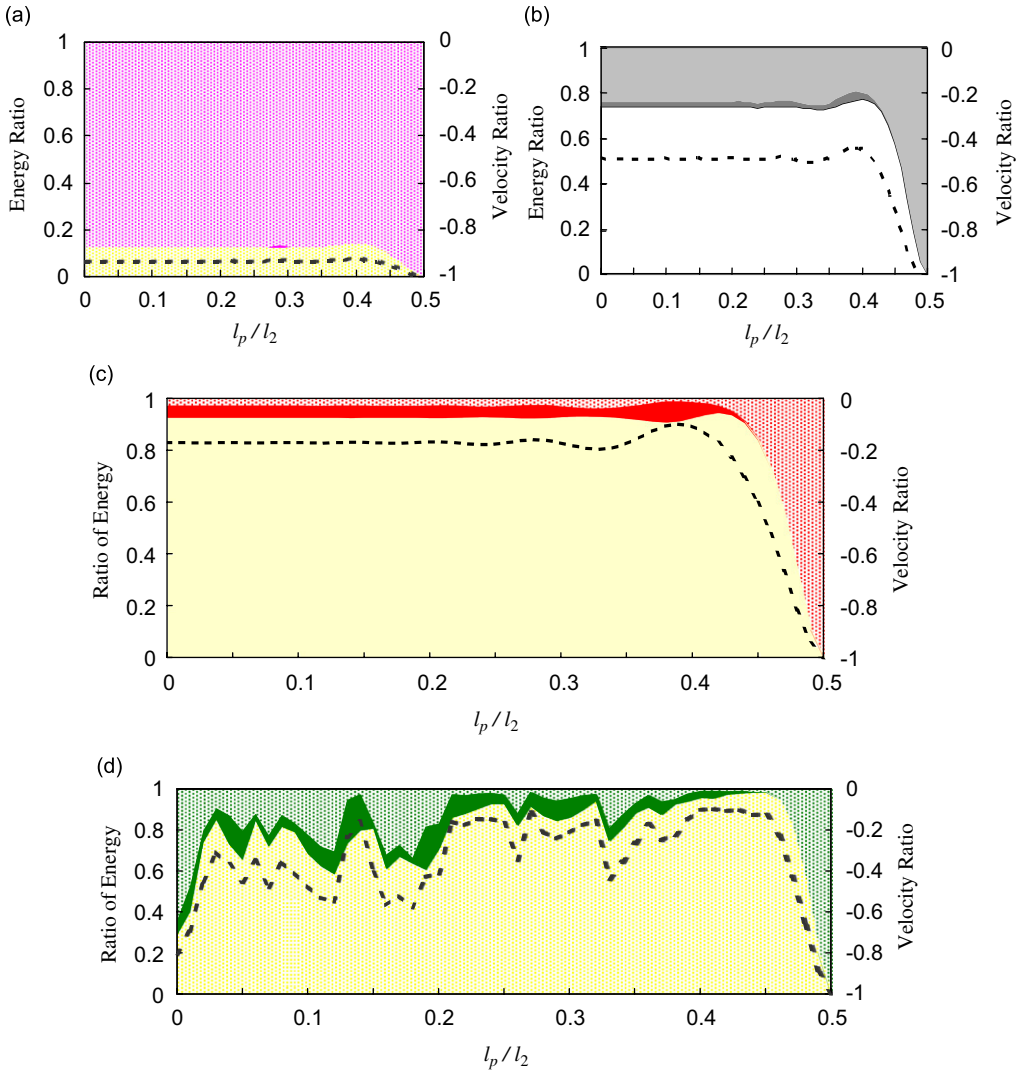

Fig. 12. Changes in mass ratio and energy distribution (theoretical) (a) $m_1/m_2 = 0.005$, (b) $m_1/m_2 = 0.025$, (c) $m_1/m_2 = 0.1$ and (d) $m_1/m_2 = 0.2$, top layer: elastic energy of beam, mid layer: elastic energy of bar, bottom layer: kinetic energy of bar, dotted line: velocity ratio (theoretical).

regardless of the position of the collision. When the ratio of natural frequencies is increased while the mass ratio is kept constant, the proportion of the elastic energy of the beam increases (Fig. 11). When the ratio of natural frequencies is kept constant and the mass ratio m_1/m_2 is gradually increased, the proportion of elastic energy of the beam again increases (Fig. 12).

In the case of one collision, there is a position, in the vicinity of the supporting point, where the elastic energies of both the beam and the bar slightly increase, the kinetic energy of the bar decreases, and the restitution of the bar becomes poor, when either the ratio of natural frequencies or the mass ratio is increased. In contrast, for intermittent-type collisions, the phenomenon is much more complicated, and the restitution condition and the energy distribution condition tend to vary with the change in parameters. However, in the vicinity of the supporting point, there is a position where the elastic energies of both the bar and the beam increase, and the kinetic energy of the bar becomes small leading to difficulty in rebounding, as is observed in the case of one collision. In the case of n collisions, even if the restitution velocity is identical, the state of elastic energy distribution can be different between the bar and the beam.

4.5. Effects of collision position and of high-order vibration of beam

Fig. 13 shows the relationships between the ratios of the maximum amplitudes of the second- and higher-order vibrations to that of the first-order vibrations of the beam after single collision, and the energy distribution and coefficient of restitution for various collision positions l_p/l_2. At the center of the beam, the even-order vibrations become nodes, and therefore, their amplitude is 0. As the position approaches the supporting point, the maximum amplitude of higher-order vibration approaches that of the first-order vibrations. With the increasing effect of the higher-order vibrations, the movement of the beam changes significantly. Therefore, it is considered that the pattern of impact force changes greatly.

Fig. 14 shows the Theoretical relationship between the number of collisions and the energy distribution condition at the center and in the vicinity of the supporting point. The circles ○ indicate the analytical nondimensionalized restitution velocity ratios obtained by calculating Eq. (16), + and − symbols indicate the velocities of the bar approaching and receding from the beam, respectively. The bar graph shows the energy distribution, with the kinetic energy of the bar, elastic energy of the bar and elastic energy of the beam shown from the top to the bottom. When the bar collides with the beam at the center, as shown in Fig. 14(a), the proportion of elastic energy of the beam decreases and that of the kinetic energy increases with increasing number of collisions. The elastic energy of the bar can either increase or decrease with increasing number of collisions. An example of the energy distribution in the vicinity of the supporting point (Fig. 14(b)) indicates that the proportion of elastic energy of the beam changes negligibly with increasing number of collisions.

5. Conclusions

1. The effectiveness of our analytical and experimental methods has been confirmed, since the theoretical and experimental impact force patterns and restitution velocities resulting from the motion of the bar

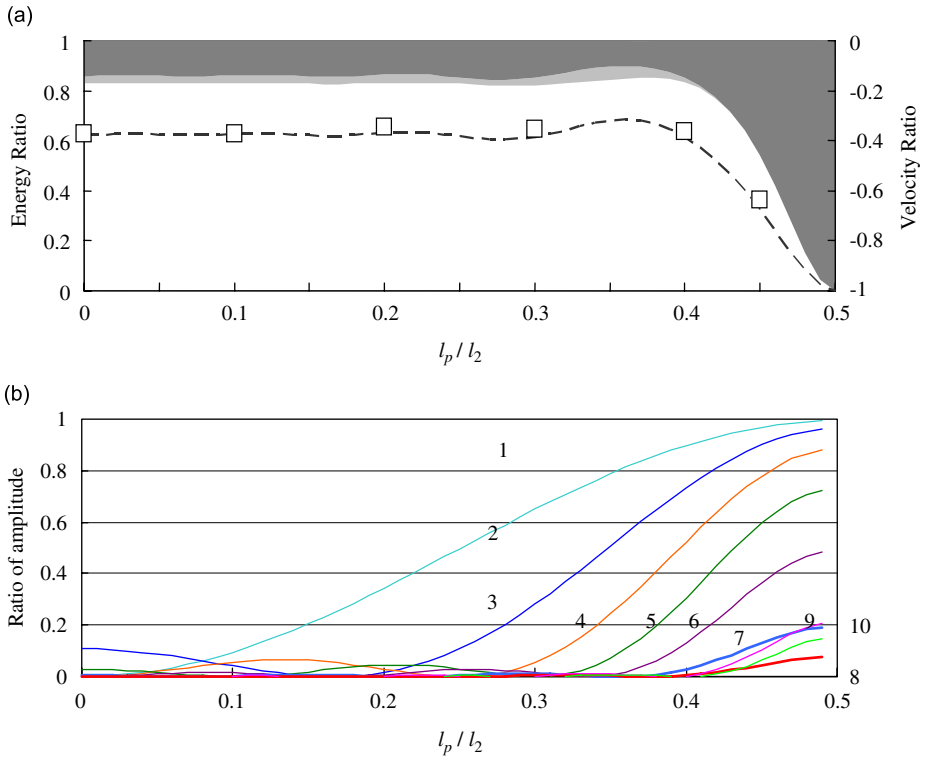

Fig. 13. Energy distribution in the case of one collision and effect of higher-order mode vibrations of the beam on energy distribution state. $n_{11}/n_{21} = 59.0$, $m_1/m_2 = 0.085$, bar: 13 mm diameter × 520 mm length (aluminum), beam: 50 mm × 10 mm × 520 mm (steel), dotted line: velocity ratio (theoretical), □: velocity ratio (experimental).

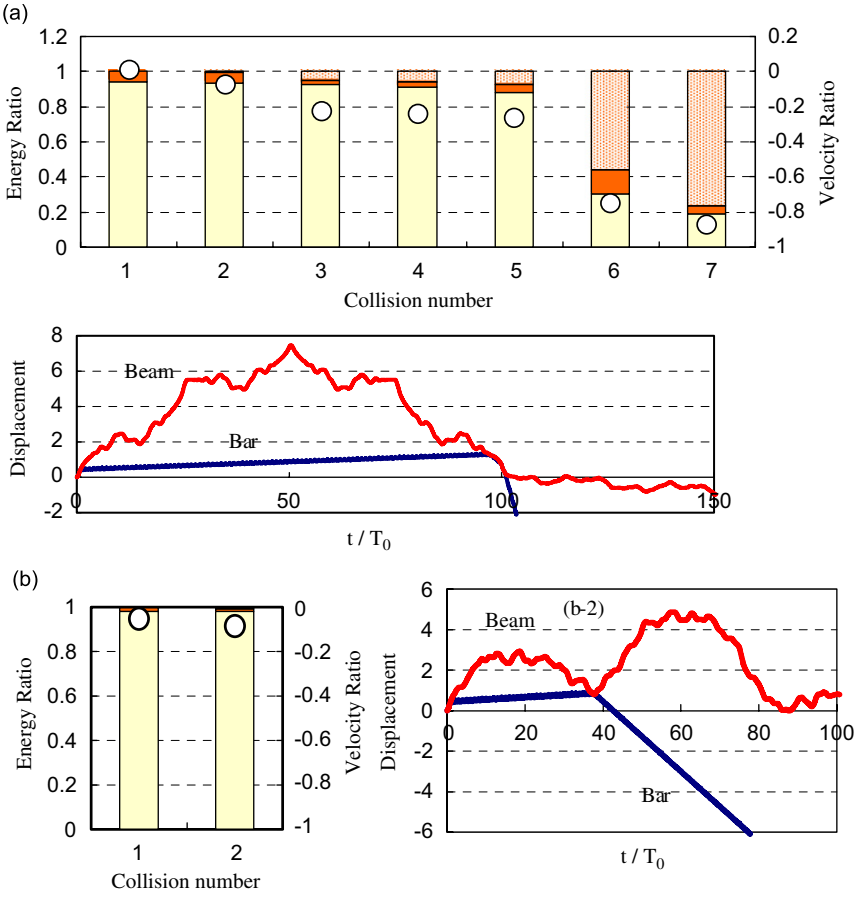

Fig. 14. Theoretical energy distribution and collision process for each collision: (a) $n_{11}/n_{21} = 200$, $m_1/m_2 = 0.1$, $l_p/l_2 = 0$ (center). (a-1) Effect of collision number on energy ratio and velocity ratio. (a-2) Displacement pattern of bar and beam. (b) $n_{11}/n_{21} = 200$, $m_1/m_2 = 0.1$, $l_p/l_2 = 0.45$ (vicinity of the supporting point). (b-1) Effect of collision number on energy ratio and velocity ratio. (b-2) Displacement pattern of bar and beam. In (a-1) and (b-1), top layer shows kinetic energy of bar, mid layer shows elastic energy of bar and bottom layer shows elastic energy of beam. ○: Velocity ratio.

and the beam are in good agreement, under various natural frequency ratios, mass ratios and collision positions.

2. The apparent coefficient of restitution is determined from (1) the natural frequency ratio of the bar and beam f_1/f_2, (2) the mass ratio of the bar and beam M_1/M_2 and (3) the collision position ratio l_p/l_2. When two bar and beam systems have the same parameter values, their restitution velocities are the same if their collision velocities are the same, regardless of the material and dimensions of the bar and beam used.
3. When a bar collides with a beam once, the proportions of elastic energies remaining in the bar and transferred to the beam increase and the proportion of the kinetic energy of the bar decreases with increasing natural frequency ratio and mass ratio.
4. For intermittent collisions, because the number of collisions and the collision process differ depending on the collision position, the proportion of elastic energy remaining in the bar and proportion of elastic energy transferred to the beam for a particular collision position differs even when the restitution velocities is the same.
5. For the energy distribution process during intermittent collisions, the elastic energy of the beam is converted into the elastic energy and kinetic energy of the bar at the center of the beam, whereas at the vicinity of the supporting point, the conversion of energy is limited and most of the elastic energy of the beam remains unchanged.

6. For both single and intermittent collisions, there is a position in the vicinity of the supporting point where the elastic energy of the beam increases and the restitution (rebound) velocity of the bar decreases. If the collision position ultimately approaches the supporting point, a slight change in the collision position will lead to a significant change in the restitution velocity, because the restitution velocity of the bar increases.
7. For intermittent collisions, the change in the energy distribution state is substantial depending on the collision position, accordingly, the restitution velocity of the bar changes. Therefore, the restitution velocity of the bar, which depends on the collision position, varies.
8. In the vicinity of the supporting point, there is a collision position where the proportions of the elastic energies of the bar and the beam are large and those of the kinetic energies are small for one collision. For intermittent collisions, there is a collision position where most of the energy is composed of the elastic energy of the beam.
9. The changes in the restitution velocity and energy state in the vicinity of the supporting point may be caused partially by the significant effect of the second- and higher-order vibrations as well as that of the first-order vibration.

Acknowledgments

I would like to express my deep gratitude to the late Dr. Genrokuro Nishimura and the late Dr. Yasuo Jimbo for initiating this research. I would also like to thank Mr. Naobumi Uchijima of Kirin Techno-System Corporation for his assistance in creating the analysis program.

References

[1] S.P. Timoshenko, *Zeitschrift fuer Mathematic und Physik* 62 (1914) 198–209.
[2] J. Tuji, M. Nishida, RIKEN Report, Vo1. 15(19), 1936, pp. 905–922.
[3] H. Matsumoto, I. Nakahara, M. Kimura, *Journal of The Japanese Society for Non-Destructive Inspection* 31 (4) (1982) 258–265.
[4] T. Shibuya, T. Koizumi, J. Tsuda, T. Okuya, *Journal of The Japanese Society for Non-Destructive Inspection* 25 (12) (1976) 795–801.
[5] G. Nishimura, T. Narabayashi, H. Sekiyama, *Proceedings of Japan Academy* 60 (9) (1984) 332–336.
[6] T. Narabayashi, A. Ishizaka, K. Ozaki, *Proceedings of the International Conference on Advanced Technology in Experimental Mechanics'99 (A.T.E.M.'99), Japan Society of Mechanical Engineers (JSME)* 1 (1999) 246–251.
[7] T. Narabayashi, N. Uchijima, A. Ishizaka, K. Ozaki, *Proceedings of the 12th International Conference on Experimental Mechanics "Advances in Experimental Mechanics (ICEM12)"*, McGraw-Hill, New York, 2004, pp.186–187.
[8] V.I. Babitsky, *Theory of Vibro-impact Systems and Applications (Foundations of Engineering Mechanics)*, Springer, Berlin, 1998, pp. 4–5.
[9] T. Narabayashi, Y. Jimbo, *Transactions of The Japan Society of Mechanical Engineers (JSME(C))* 56 (532) (1990) 3233–3239.